JGR Space Physics

RESEARCH ARTICLE
10.1029/2023JA032240

Lower Band Chorus Wave Scattering Causing the Extensive Morningside Diffuse Auroral Precipitation During Active Geomagnetic Conditions: A Detailed Case Study

Huiting Feng[1,2], Dedong Wang[2], Deyu Guo[3], Yuri Y. Shprits[2], Desheng Han[1], Shangchun Teng[1], BinBin Ni[3,4], Run Shi[1], and Yongliang Zhang[5]

[1]State Key Laboratory of Marine Geology, School of Ocean and Earth Science, Tongji University, Shanghai, China, [2]Section 2.7 Space Physics and Space Weather, GFZ German Research Centre for Geosciences, Potsdam, Germany, [3]Department of Space Physics, School of Electronic Information, Wuhan University, Wuhan, China, [4]CAS Center for Excellence in Comparative Planetology, Hefei, China, [5]The Johns Hopkins University Applied Physics Laboratory, Laurel, MD, USA

Abstract The diffuse aurora is a natural phenomenon observed over the Earth's polar region. Compared with the nightside diffuse aurora, the brightness of the dayside diffuse aurora (0600–1800 magnetic local time (MLT)) is relatively weak, thus requiring more stringent observation conditions. Therefore, the current understanding of what causes the dayside diffuse aurora is still quite limited. Here, we present an intense morningside diffuse aurora (0600–1000 MLT) event observed on 1 January 2016 during the recovery phase of the substorm, using conjugate observations of wave and particle spectrum from the Radiation Belt Storm Probes and auroral emission from the Special Sensor Ultraviolet Spectrographic Imagers on the Air Force Defense Meteorological Satellite Program (DMSP/SSUSI). We perform calculations of diffusion coefficients and simulations of the electron fluxes for this event. Our results show that the chorus waves are the primary contributors to the formation of the morningside diffuse aurora, with precipitated electron energies ranging from a few keV to tens of keV. The lower band chorus shows significant pitch angle scattering efficiency for electrons with energies from 5 to 20 keV. The upper band chorus waves induce acceleration effects on 1–20 keV electrons. We suggest that the upper band chorus waves accelerate low-energy electrons to higher energies, enabling them to engage in the scattering process of the lower band chorus waves. Our study makes a contribution to recent research on the formation mechanisms of diffuse aurora and deepens our understanding of wave-particle interactions leading to dayside electron precipitation.

Key Points:

- We present observations of an intense morningside diffuse aurora accompanied by chorus wave activity during disturbed geomagnetic conditions
- Lower band chorus waves scatter electrons with energies >5 keV during this event, causing morningside diffuse aurora
- Upper-band chorus waves accelerate 1–20 keV electrons, and therefore also participate in the scattering process

Correspondence to:
D. Wang,
dedong.wang@gfz-potsdam.de

Citation:
Feng, H., Wang, D., Guo, D., Shprits, Y. Y., Han, D., Teng, S., et al. (2024). Lower band chorus wave scattering causing the extensive morningside diffuse auroral precipitation during active geomagnetic conditions: A detailed case study. *Journal of Geophysical Research: Space Physics*, *129*, e2023JA032240. https://doi.org/10.1029/2023JA032240

Received 30 OCT 2023
Accepted 5 APR 2024

Author Contributions:
Conceptualization: Huiting Feng, Dedong Wang, Deyu Guo, Yuri Y. Shprits, Desheng Han, Shangchun Teng, Run Shi
Data curation: Huiting Feng, Dedong Wang, Deyu Guo, Shangchun Teng, Yongliang Zhang
Formal analysis: Huiting Feng, Dedong Wang, Deyu Guo, Yuri Y. Shprits
Funding acquisition: Dedong Wang, Yuri Y. Shprits, Desheng Han, Shangchun Teng, BinBin Ni
Investigation: Huiting Feng, Dedong Wang, Deyu Guo
Methodology: Huiting Feng, Dedong Wang, Deyu Guo, Yuri Y. Shprits, Desheng Han, Shangchun Teng, BinBin Ni, Run Shi
Project administration: Dedong Wang, Desheng Han

1. Introduction

Aurorae are the ionospheric manifestation of the coupling process between the solar wind and Earth's magnetosphere. Most of them occur in the oval-shaped regions centered on the magnetic poles, called auroral ovals (Feldstein, 1973, 2016), and they can also be observed in the polar cap surrounded by the poleward edges of the auroral oval at some specific conditions (e.g., Feng et al., 2021; Han et al., 2020; Hosokawa et al., 2020; Kullen, 2012). Based on their different optical characteristics and generation mechanisms, aurorae can be divided into discrete aurora and diffuse aurora (e.g., Feldstein & Galperin, 1985; Frank & Ackerson, 1972; Lui et al., 1975). Diffuse aurorae typically appear as hazy emissions with undiscernible patterns or structures, which are usually observed in the equatorward portion of the auroral oval over a broad latitude range (Lui et al., 1973). This region spans a latitude range of 5°–10° and maps the entire central plasma sheet (CPS) along geomagnetic field lines. Under the combined action of $E \times B$ and gradient forces, the energetic particles originating from the CPS with energies ranging from 0.1 to 30 keV will drift toward the dayside. During this process, they interact with certain waves and are scattered into the ionosphere, forming the diffuse aurora (e.g., Lyons, 1974; Swift, 1981; Thorne, 2010). Therefore, the diffuse aurora is most intense at midnight, gradually weakens toward the local noon, and tends to be relatively unnoticeable from post-noon to dusk sectors. Under moderate geomagnetic activity conditions (Kp ~3), the diffuse aurora can extend to more dayside and low-latitude regions. It can be observed at all magnetic local times under more active geomagnetic conditions (Royrvik & Davis, 1977).

The Earth's magnetosphere is host to various plasma waves, such as whistler mode waves, electromagnetic ion cyclotron waves, electron cyclotron harmonic (ECH) waves et al. (e.g., Li et al., 2009; Ma et al., 2019; Min et al., 2012; Teng, Li, et al., 2019; Thorne et al., 2010; Wang et al., 2016). These waves interact with radiation belt

Resources: Dedong Wang, Deyu Guo, Yuri Y. Shprits, Desheng Han, Shangchun Teng, Yongliang Zhang
Software: Huiting Feng, Dedong Wang, Deyu Guo, Yuri Y. Shprits, Desheng Han, Shangchun Teng, BinBin Ni, Run Shi
Supervision: Dedong Wang, Yuri Y. Shprits, Desheng Han, Shangchun Teng, BinBin Ni, Run Shi
Validation: Huiting Feng, Dedong Wang, Deyu Guo, Yuri Y. Shprits, Shangchun Teng
Visualization: Huiting Feng, Dedong Wang, Deyu Guo
Writing – original draft: Huiting Feng, Dedong Wang, Deyu Guo
Writing – review & editing: Huiting Feng, Dedong Wang, Deyu Guo, Yuri Y. Shprits, Desheng Han, Shangchun Teng, BinBin Ni, Run Shi

electrons, affecting the dynamics of charged particles in the magnetosphere (e.g., Baker, 2021; Lyons & Thorne, 1973; Li & Hudson, 2019; Ripoll et al., 2020; Shprits et al., 2008a, Shprits, Thorne, et al., 2006; Thorne et al., 2010). In particular, ultralow frequency waves are widespread in the magnetosphere, transporting electrons radially outward or inward by radial diffusion (e.g., Elkington, 2006; Shprits, Thorne, et al., 2006). Whistler mode chorus is mainly observed in the low-density region outside the plasmapause from midnight to the post noon sectors, manifesting as both a lower band with a frequency ranging from 0.05 electron cyclotron frequency (f_{ce}) to 0.5 $f_{ce,}$ and an upper band with a frequency ranging from 0.5 f_{ce} to f_{ce}, with a distinct gap near 0.5 f_{ce}, where f_{ce} is the equatorial gyrofrequency of electrons (e.g., Burtis & Helliwell, 1969; Gao et al., 2019; Teng, Tao, & Li, 2019; Tsurutani & Smith, 1974). Chorus waves are known to accelerate radiation belt electrons to relativistic energies, and precipitate electrons into the upper atmosphere through pitch angle scattering (e.g., Bortnik & Thorne, 2007; Shprits et al., 2008b; Thorne et al., 2010). The ECH waves are excited near the geomagnetic equator and appear as multiple harmonic bands, distributed throughout the outer magnetosphere ($L > 5$) from nightside to dayside during the active geomagnetic conditions (e.g., Horne et al., 1981; Kennel et al., 1970; Ni et al., 2012). The typical energy of ECH resonant particles ranges from a few hundred eV to several keV (e.g., Horne & Thorne, 2000; Horne et al., 2003).

The exact wave modes causing the diffuse aurora and the specific physical processes have been a subject of ongoing investigation. Currently, studies suggest that the electrostatic ECH waves and whistler mode chorus waves are the two main candidates for scattering particles from the plasma sheet into the loss cone (e.g., Ni & Thorne, 2012; Ni et al., 2016; Nishimura et al., 2020; Lou et al., 2021). Thorne et al. (2010) show that both ECH waves and chorus waves increase in intensity as geomagnetic activity intensifies, and this intensification is accompanied by the enhancement of average diffuse aurora emission from 2 to 12 keV. Numerous prior studies show that both kinds of waves play an important role in generating diffuse aurora in different regions of the magnetosphere (e.g., Ni & Thorne, 2012; Nishimura et al., 2020; Teng et al., 2023). At the nightside in the inner magnetosphere, chorus waves are suggested to be the dominant contributor, which is firmly supported by both observational and simulated results (e.g., Ni & Thorne, 2012; Nishimura et al., 2020). For instance, Thorne et al. (2010) conducted extensive theoretical and modeling studies based on NASA Combined Release and Radiation Effects Satellite (CRRES) observations, and found that the chorus waves have a profound effect on the overall electron population injected into the inner magnetosphere, leading to a pancake distribution at energies below a few keV. Using joint in situ- and ground-observations in Time History of Events and Macroscale Interactions during Substorms (THEMIS) satellites, Nishimura et al. (2010) provided direct evidence that the modulation by chorus waves drives the pulsating aurora, which are a type of diffuse aurorae, with an almost one-to-one intensity correspondence with each chorus burst. With the observations from the Reimei satellite, Miyoshi et al. (2015) found that the brightness of pulsating aurora shows good correlation with higher energy electron precipitation, while general diffuse aurorae are well correlated with increased precipitation of lower energy electrons, which they attributed to the presence of lower and upper band chorus waves. However, it is not clear yet in which region chorus waves dominate the auroral electron precipitation and in which region ECH waves dominate. At the nightside in the outer magnetosphere ($L > \sim 8$), the ECH waves are thought to be an important contributor (e.g., Ni & Thorne, 2012; Yamamoto, 1988). Liang et al. (2010, 2011) performed detailed case studies that combined THEMIS and ground-based NORSTAR optical auroral observations and showed a positive correlation between the intensity of diffuse aurora precipitation and ECH emission. Later, Ni et al. (2012) conducted a thorough theoretical and numerical analysis of the resonant scattering rate driven by ECH waves for the event reported by Liang et al. (2011) and revealed that the observed ECH wave activity leads to significant pitch angle scattering of plasma sheet electrons, resulting in diffuse aurora.

Dayside diffuse aurorae (0600–1800 magnetic local time (MLT)) are less intense than the ones on the nightside (1800–0600 MLT), many previous studies primarily focused on the nightside, while only a few explored on the dayside diffuse aurorae due to observational limitations (e.g., Han et al., 2015; Ni et al., 2016). Using 7-year ground auroral observations from Yellow River Station, Han et al. (2015) conducted a systematic statistical on the dayside diffuse auroras and classified them into two broad types based on their optical characteristics, namely unstructured and structured dayside diffuse auroras. The dayside chorus wave is a potential contributor to dayside diffuse auroral precipitation considering the continuous presence of dayside chorus waves, as documented by Li et al. (2009). Shi et al. (2012) reported an intense dayside diffuse auroral event from ground observations near local noon at $L = \sim 9.5$. By computing bounce-average pitch angle diffusion coefficients in realistic magnetic field models, they concluded that the presence of dayside chorus during this event can result in significant precipitation

losses of electrons from CPS on timescales of hours. Using simultaneous measurements of dayside diffuse aurora and whistler-mode waves made by the South Pole all-sky imager and the THEMIS spacecraft, Nishimura et al. (2013) found a strong correlation between the intensity of diffuse aurora at 557.7 nm and whistler-mode chorus on board the THEMIS satellites at $6 < L < 11$. Ni et al. (2014) further performed a detailed quantitative analysis of wave-driven diffusion and electron precipitation for one event in Nishimura et al. (2013), and the results indicate that dayside chorus scattering is likely to play a major contributing factor to the formation of the dayside diffuse aurora during quiet geomagnetic conditions. Shi et al. (2015) reported another event in which the intensity of dayside electron diffuse aurora was modulated by the solar wind dynamic pressure, with the correlation coefficient reaching 0.89. The increase in dynamic pressure was suggested as a necessary condition for creating favorable conditions for the generation of dayside chorus waves.

Due to the limitations in observations for the dayside auroral measurements (i.e., Imager observations require the polar night season), understanding the mechanisms responsible for the generation of dayside aurora is still incomplete, and it is challenging to find favorable conjugate events for concurrent observations of in situ wave properties and auroral emission. However, observations by the Air Force Defense Meteorological Satellite Program (DMSP) and the Radiation Belt Storm Probes (RBSP) provided an opportunity to find such conjunctions during disturbed geomagnetic activity. In this paper, we show an ultraviolet diffuse aurora event observed in the morningside (0600–1000 MLT) from the Special Sensor Ultraviolet Spectrographic Imagers (SSUSI) on the DMSP satellites, combined with the wave spectra and particle observations from RBSP. Based on the observation of this event, we compute wave-driven bounce-averaged quasi-linear diffusion coefficients using Full Diffusion Code (FDC) (Ni et al., 2008; Shprits & Ni, 2009). Then we use these diffusion coefficients to solve the 2-D bounce-averaged Fokker-Planck equation for the evolution of electron fluxes, and also evaluate the electron lifetimes following Shprits, Li, and Thorne (2006) to gain a comprehensive understanding of the origin of the dayside diffuse aurora.

2. Data

The auroral data used in this paper are derived from DMSP satellites operating in a sun-synchronous orbit of ∼840 km with an orbital period of 101 min (Paxton et al., 1992). The DMSP satellite carries the SSUSI providing five wavelengths to record auroral emission, at 121.6 nm, 130.4 nm, 135.6 nm, 140–150 nm (LBHS), and 165–180 nm (LBHL) (Paxton et al., 1992). In addition, the satellite is equipped with the Special Sensor *J* (SSJ) instrument to record the energy flux of precipitating ions and electrons (Hardy et al., 1984). The wave spectrograms used for the study are retrieved from the Electric and Magnetic Field Instrument Suite (EMFISIS) (Kletzing et al., 2013) running on the RBSP satellites (probes A and B) with a high elliptical orbit of 600 km altitude, an apogee at ∼5.8 R_E, 10° inclination, and ∼9-hr orbital period (Kessel et al., 2013). The EMFISIS provides measurements of wave electric and magnetic fields with a wide frequency range, spanning from 10 Hz to 400 kHz, and a sampling cadence of 64 vectors/s (Kletzing et al., 2013). The particle data used for the study is from the Helium, Oxygen, Proton, and Electron (HOPE) Mass Spectrometers on RBSP, which measure both ions and electrons over 1 eV to 50 keV in 36 log-spaced steps (Funsten et al., 2013). The interplanetary magnetic field data used in this study are extracted from the National Aeronautics and Space Administration/Goddard Space Flight Center (NASA/GSFC)'s OMNI data set.

3. Conjugate Measurement of Morningside Diffuse Aurora and In Situ Wave Observations on 1 January 2016

We report a morningside diffuse aurora event associated with chorus wave activity, jointly observed by the DMSP and RBSP-B on 1 January 2016 during the recovery phase of a substorm. Figures 1a and 1b show the solar wind dynamic pressure and geomagnetic indices from 0700 UT to 1100 UT derived from OMNI 1-min data. During this period, the geomagnetic condition is relatively active, accompanied by substorm events (Kp index changes from 5 to 3, not shown here). Additionally, there is an enhancement in dynamic pressure from ∼0.5 to ∼1.5 nPa at ∼0900 UT, as indicated in the red arrow in Figure 1a. During the substorm recovery phase, as shown in the red-shaded region in Figure 1, we observe a strong morningside diffuse aurora precipitation event at DMSP/SSUSI, as shown in Figure 1c. The DMSP F17 satellite flies from duskside to dawnside, denoted with a red line in Figure 1c. From 1008 UT to 1012 UT, the F17 satellite is in the intense morningside diffuse aurora region, and coincidentally, the footprints of RBSP-b mapped by the T89 magnetic model (Tsyganenko, 1989) align perfectly with this zone, denoted by the green line in Figure 1c. Figures 1d and 1e show the energy flux spectra of electrons and

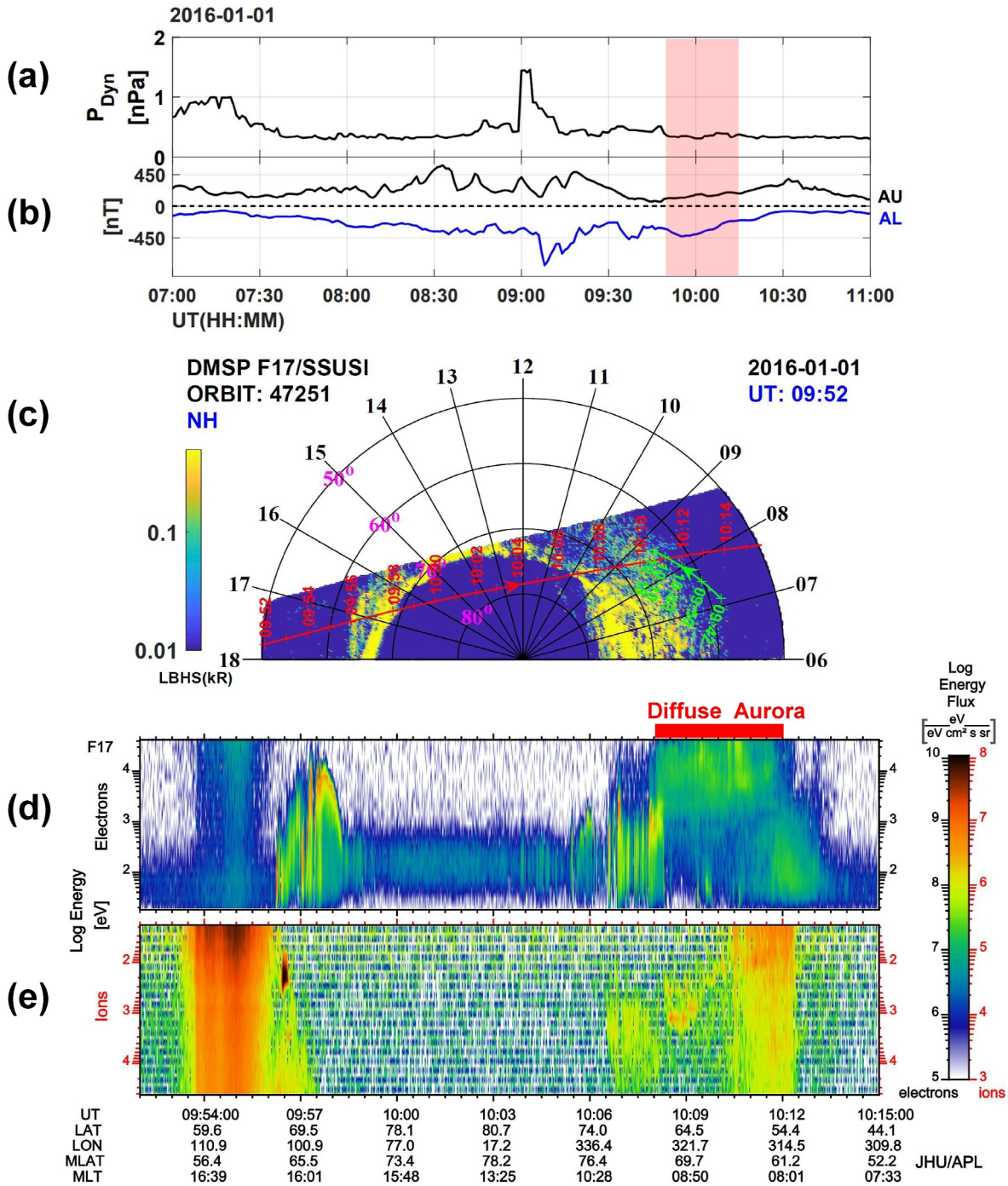

Figure 1. The conjugate observation of morning-side diffuse aurora by Defense Meteorological Satellite Program (DMSP) and RBSP-B on 1 January 2016. (a) The variation of solar wind dynamic pressure. (b) The geomagnetic AU and AL indices. (c) The auroral emission observations in LBHS wavelength from DMSP/SSUSI. The red arrow line shows the trajectory of the DMSP and the green arrow line is the footprint of RBSP-b mapped by the T89 magnetic model. (d) and (e) The energy flux spectrum of electrons and ions taken from the Special Sensor J instrument on DMSP (Note that the energy scale for ions is the opposite of that for electrons).

ions recorded by the SSJ instrument on DMSP F17. In the diffuse auroral region, the flux of electrons is relatively uniformly distributed at high energy levels (from 1 keV to tens of keV) and shows low flux at lower energy levels (<1 keV). The energy of precipitated ions ranges from tens to hundreds of eV (Note that the energy scale for ions is the opposite of that for electrons). These particles are suggested to be from the CPS (Wing & Newell, 1998).

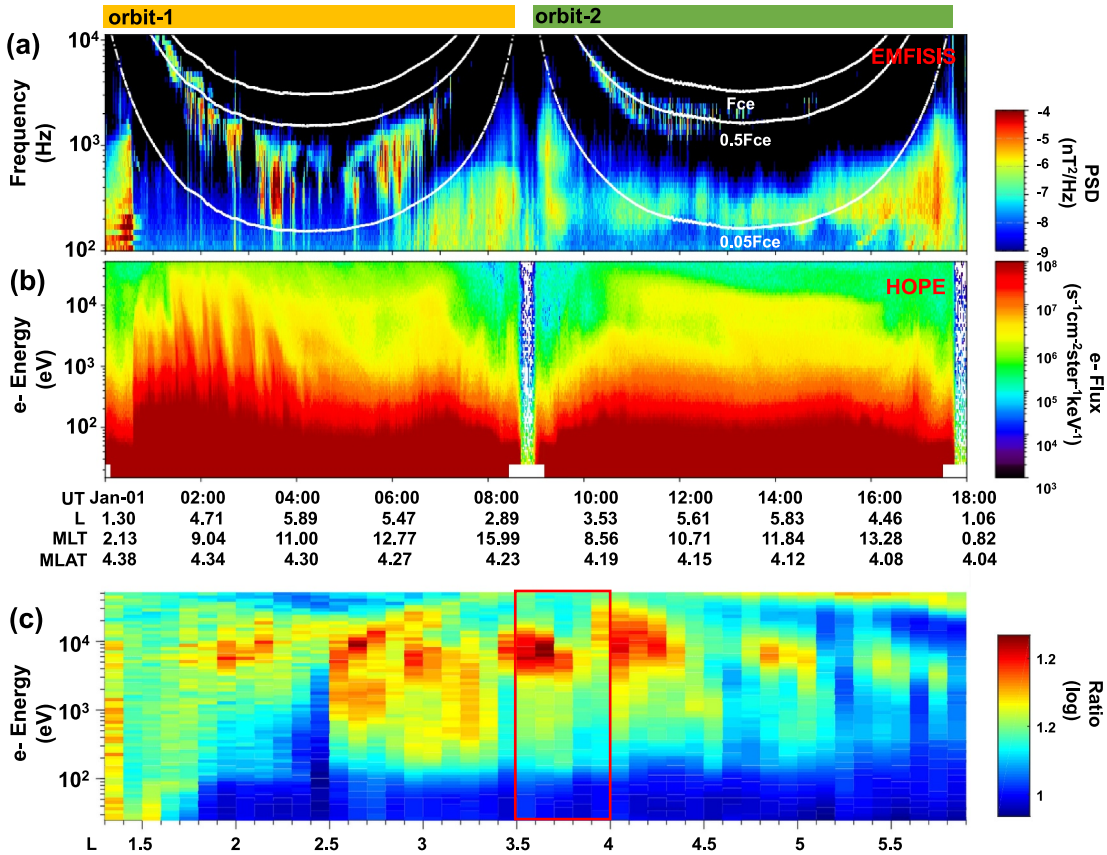

Figure 2. The wave spectra and the electron energy flux distribution of RBSP-b from 0000 UT to 1800 UT on 1 January 2016. (a) The chorus wave spectra on the EMFISIS instrument. The white curves indicate 0.05-, 0.5-, and 1-times f_{ce} calculated by the equatorial magnetic field. (b) The electron energy flux distributions on the Helium, Oxygen, Proton, and Electron instrument. (c) The ratio of energy flux spectra of the first half of orbit-1 and orbit-2. The red box indicated the time period of conjugate observation of diffuse aurora by Defense Meteorological Satellite Program and RBSP-b.

Figure 2 shows the wave spectra and particle distribution observations from RBSP-B on 1 January 2016. Figure 2a presents the chorus wave spectra extracted from the EMFISIS instrument, with the white curves indicating the 0.05, 0.5-, and 1-times the electron cyclotron frequency (f_{ce}) calculated from the equatorial magnetic field. From 0000 UT to 1800 UT, as the satellite traversed the same region along its pre-orbit (from ~0000 to ~0900 UT) and post-orbit (from ~0900 to ~1800 UT) (hereafter we will refer to them as orbit-1 and orbit-2), chorus waves of different intensities are observed. During orbit-1, RBSP-b first observed both the upper and lower band chorus, with the lower band chorus taking on a dominant role. However, the chorus waves are less intense in orbit-2 than in orbit-1, with both the upper band and lower band chorus present. Figure 2b shows the electron energy flux recorded by the HOPE instrument on RBSP-b. We can see that the electron flux is more concentrated on low energy levels (<1 keV) during this period. However, at relatively high energy levels ranging from 1 keV to tens of keV, higher electron fluxes are observed during the preceding phase of orbit-1 compared to orbit-2 (i.e., 0000–0400 UT and 0900–~1300 UT). To further confirm which energy level electrons are mainly reduced, we initially reconstructed the full electron energy flux matrix for the first half of orbit-1 and orbit-2, with the step size of L as 0.1, and calculated the average flux for each energy level. Subsequently, we plot the ratio spectrum (orbit-1/orbit-2), as illustrated in Figure 2c. We can see an obvious decrease in the flux of the particles with ~5–~20 keV energies during the period that diffuse aurorae are observed (L is roughly from 3.5 to 4, UT = 1,000–1,018), which is consistent with these diffuse aurorae associated with the precipitation electron with several keV to tens of keV observed by DMSP, as shown in Figure 1.

4. Simulation Methods and Results

In this section, we perform quantitative analysis to confirm whether the morning-side diffuse aurora observed in DMSP/SSUSI is associated with the chorus waves observed in RBSP-b in this case. We first compute the bounce-

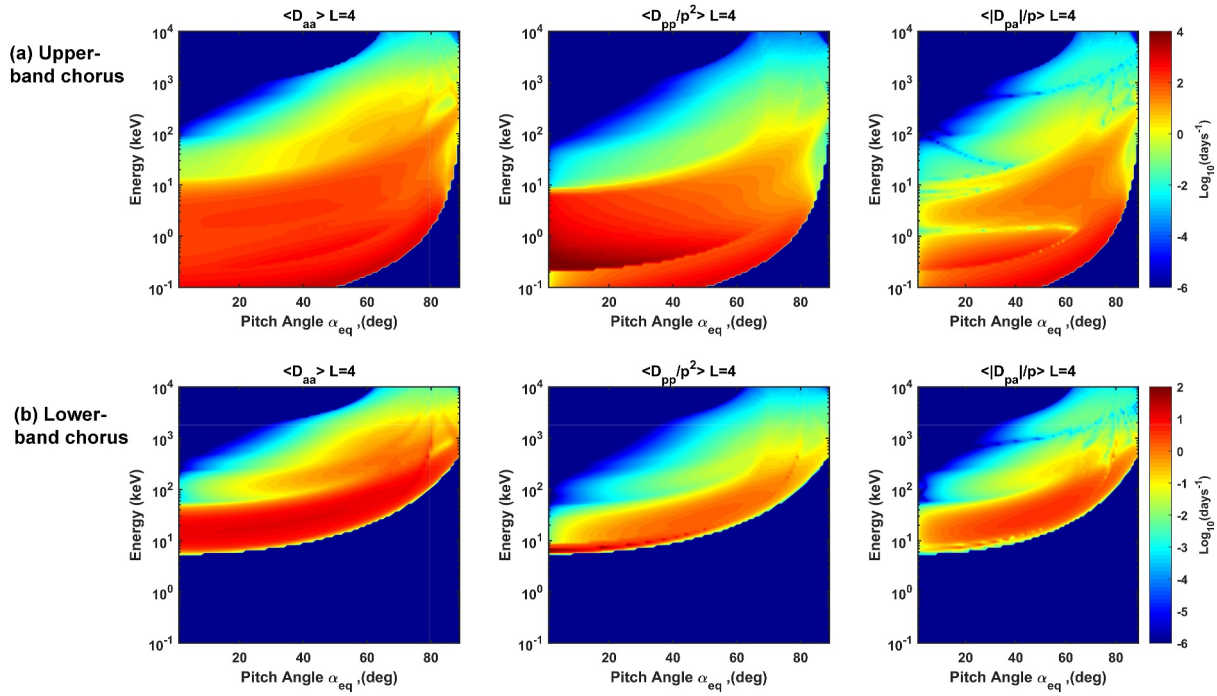

Figure 3. The bounce-averaged diffusion rates of electrons are between 10^{-1} keV and 10^{4} keV. The panels in the first and second rows (a) and (b) indicate the pitch angle, momentum, and cross-pitch angle-momentum diffusion coefficients contributed from the upper band chorus and lower band chorus, respectively.

averaged pitch-angle and momentum diffusion coefficients using chorus waves observed by RBSP-b and a dipole magnetic field model. Then, we simulate the temporal evolution of electrons in the inner magnetosphere based on the average scattering rates derived from the diffusion coefficients, together with real electron distributions observed by RBSP-b/HOPE, as shown in Figure 2b.

To analyze the interaction between chorus wave and morning-side diffuse aurora on this day, we calculate the bounce averaged quasi-linear diffusion coefficients in pitch angle ($\langle D_{\alpha\alpha}\rangle$), momentum ($\langle D_{pp}\rangle$), and cross pitch angle-momentum ($\langle D_{\alpha p}\rangle = \langle D_{p\alpha}\rangle$) using the FDC (Ni et al., 2008; Orlova & Shprits, 2011; Shprits & Ni, 2009; Shprits et al., 2009). We assume that the chorus wave power spectral density $B^2(f)$ is distributed following the Gaussian frequency distribution with lower bounds (f_{lc}), upper bounds (f_{uc}), median value (f_m), and bandwidth (δf):

$$B^2(f) = B_W^2 \frac{2}{\sqrt{\pi}\delta f}\left[\mathrm{erf}\left(\frac{f_m - f_{lc}}{\delta f}\right) + \mathrm{erf}\left(\frac{f_{\mathrm{uc}} - f_m}{\delta f}\right)\right]^{-1} \exp\left[-\left(\frac{f - f_m}{\delta f}\right)^2\right] \quad (1)$$

B_W^2 is the chorus wave amplitude and erf is the error function. Based on the observations of the time and L-values at which diffuse aurora and chorus occurred, we identify the f_{lc}, f_{uc}, f_m, and B_W from the real chorus wave spectra observed within the L-value range of 3.9–4.1 in orbit-1. We perform calculations separately for the lower band chorus and upper band chorus. The parameters for lower band chorus are $f_{lc} = 0.3f_{\mathrm{ce}}$, $f_{\mathrm{uc}} = 0.5f_{\mathrm{ce}}$, $f_m = 0.4f_{\mathrm{ce}}$, and $B_W = 23.7$ pT, and for upper-band chorus are $f_{lc} = 0.5f_{\mathrm{ce}}$, $f_{\mathrm{uc}} = 0.7f_{\mathrm{ce}}$, $f_m = 0.6f_{\mathrm{ce}}$, and $B_W = 43.27$ pT. Plasma density is about 20 cm^{-3}, derived from RBSP-b observations. Waves are assumed to exist only within 10° from equator ($\lambda_m = 10^{\circ}$).

Figure 3 shows the bounce-averaged diffusion rates of electrons between 10^{-1} keV and 10^{4} keV from the upper band chorus and lower band chorus contributions separately. The pitch angle diffusion coefficients ($\langle D_{\alpha\alpha}\rangle$) for upper band chorus waves and lower band chorus waves show that near the loss cone, the upper band chorus induce intense pitch-angle scattering of electrons with energies ranging from 0.1 to ∼50 keV. The scattering is most pronounced at energies below 10 keV. The lower band chorus can cause efficient pitch angle scattering of electron between 3 and ∼100 keV, and is most intense for ∼10 keV. There is less efficient electron scattering for $\alpha_{eq} >$ ∼80°, which can explain the formation of a pancake shape pitch angle distribution (e.g., Meredith

et al., 1999). Calculation results show that the upper band chorus waves lead to large momentum diffusion coefficients for electrons with energies below ~20 keV, while the lower band chorus waves lead to large momentum diffusion coefficients for electron energies varying from ~3 to ~200 keV.

The morning-side diffuse aurora observed by DMSP is mainly produced by electrons with energy higher than 1 keV, especially those of tens of keV, as shown in Figure 1. However, both the upper band chorus and lower band chorus exhibit the ability to scatter the electrons in the energy range from several keV to tens of keV. The noticeable difference between them is that the upper band chorus has more effective scattering rates for relatively low-energy electrons (<10 keV), and the lower band chorus has intense scattering rates for relatively high-energy electrons (3–30 keV). Therefore, further analysis is needed to quantify the contribution from each. We thus model the evolution of electron phase space density (PSD) f by solving the following 2-D bounce-averaged Fokker-Planck equation at a fixed L shell (here, $L = 4$) using the diffusion coefficients computed above (e.g., Albert, 2004; Kozyra et al., 1994; Shprits et al., 2008b; Xiao et al., 2009),

$$\frac{\partial f}{\partial t} = \frac{1}{Gp}\frac{\partial}{\partial \alpha_e}\left[G\left(\hat{D_{\alpha\alpha}}\frac{1}{p}\frac{\partial f}{\partial \alpha_e} + \hat{D_{\alpha p}}\frac{\partial f}{\partial p}\right)\right] + \frac{1}{G}\frac{\partial}{\partial_p}\left[G\left(\hat{D_{p\alpha}}\frac{1}{p}\frac{\partial f}{\partial \alpha_e} + \hat{D_{pp}}\frac{\partial f}{\partial p}\right)\right] \quad (2)$$

where p is the electron momentum, $G = p^2T(\alpha_e)\sin\alpha_e\cos\alpha_e$, the normalized bounce time $T(\alpha_e) \approx 1.30–0.56\sin\alpha_e$. The boundary conditions for PSD in α_{eq} space are $f(\alpha_{eq} \le \alpha_{LC}) = 0$ and $\frac{\partial f}{\partial \alpha_{eq}}(\alpha_{eq} = 90°) = 0$ where α_{LC} is equatorial bounce loss cone (for $L = 4$ here, $\alpha_{LC} = 5.34^{\circ}$). Phase space density is assumed to be constant at the low energy (0.1 keV) boundary and high energy boundary (100 keV). The simulation was performed for 10 hr with a 1s time step. The initial condition uses the electron PSD converted from the fluxes observed by the HOPE instrument at $L = 4$ during orbit-1. We model the temporal evolution of energetic electron pitch angle distribution due to the upper band chorus, lower band chorus, and the combined effect.

Figure 4 shows the temporal variations of electron fluxes (converted from the PSD results) at five specific energies ($E = 1, 2, 5, 10, 20$ keV) for a period of 10 hr. Results are shown increasing from initial conditions ($t = 0$, indicated by blue curve) in 1-hr step to $t = 10$ hr (represented by red curves). The modeled pitch angle distributions exhibit significant differences between the contributions of the upper band chorus and lower band chorus. When only upper band chorus is included in the simulation, electrons are primarily accelerated, with the 5 keV electrons being accelerated the fastest, as shown in the second column of Figure 4. In contrast, when the lower band chorus is the main contributor, 5–20 keV electrons with low and middle pitch angles are rapidly lost, as presented in the third column of Figure 4. This is consistent with the RBSP-b electron observations showing that the ~5–~20 keV electron flux decreases at orbit-2 compared to orbit-1, as shown in Figure 2c. The combined effect causes acceleration at all electron energy levels due to the acceleration from the upper band chorus contributing most significantly (the first column in Figure 4).

To further evaluate the loss effect of the lower band chorus on energetic electrons, we computed electron lifetimes (τ_D) for 5 keV (red lines), 10 keV (blue lines) and 20 keV (green lines) electrons by only considering pitch angle diffusion due to lower band chorus waves. Here, we compare the τ_D obtained by two methods, as shown in Figure 5.

The τ_D plotted in dotted lines are estimated by using $1/D_{\alpha\alpha}$, where the $D_{\alpha\alpha}$ is evaluated at the equatorial loss cone angle $(\alpha_{eq})_{LC}$ (e.g., Shprits, Li, & Thorne, 2006; Summers et al., 2007). The τ_D shown by the solid lines are given by the formula as follows (Shprits, Li, & Thorne, 2006)

$$\tau(\alpha) = \frac{\left(f^{n+1}(\alpha) + f^{n}(\alpha)\right)dt}{2\left(f^{n}(\alpha) - f^{n+1}(\alpha)\right)} \quad (3)$$

where $f(\alpha)$ is a pitch angle distribution, dt is the time step of the simulation, and superscript n is an indicator of the simulation time step. The loss cone at $L = 4$ is assumed to be constant 5.34°. The lifetimes for all these energetic particles are short, only a few hours. Among them, the 10 keV electrons are scattered the most efficiently, with a lifetime of 0.1 days. This means that the particles injected from the plasma sheet can be quickly scattered into the atmosphere by the lower band chorus waves as they drift from midnight to morning side. As a result, this precipitation of a large number of energetic particles into the ionosphere excites the diffuse aurora over a large area on the morningside, as shown in Figure 1c.

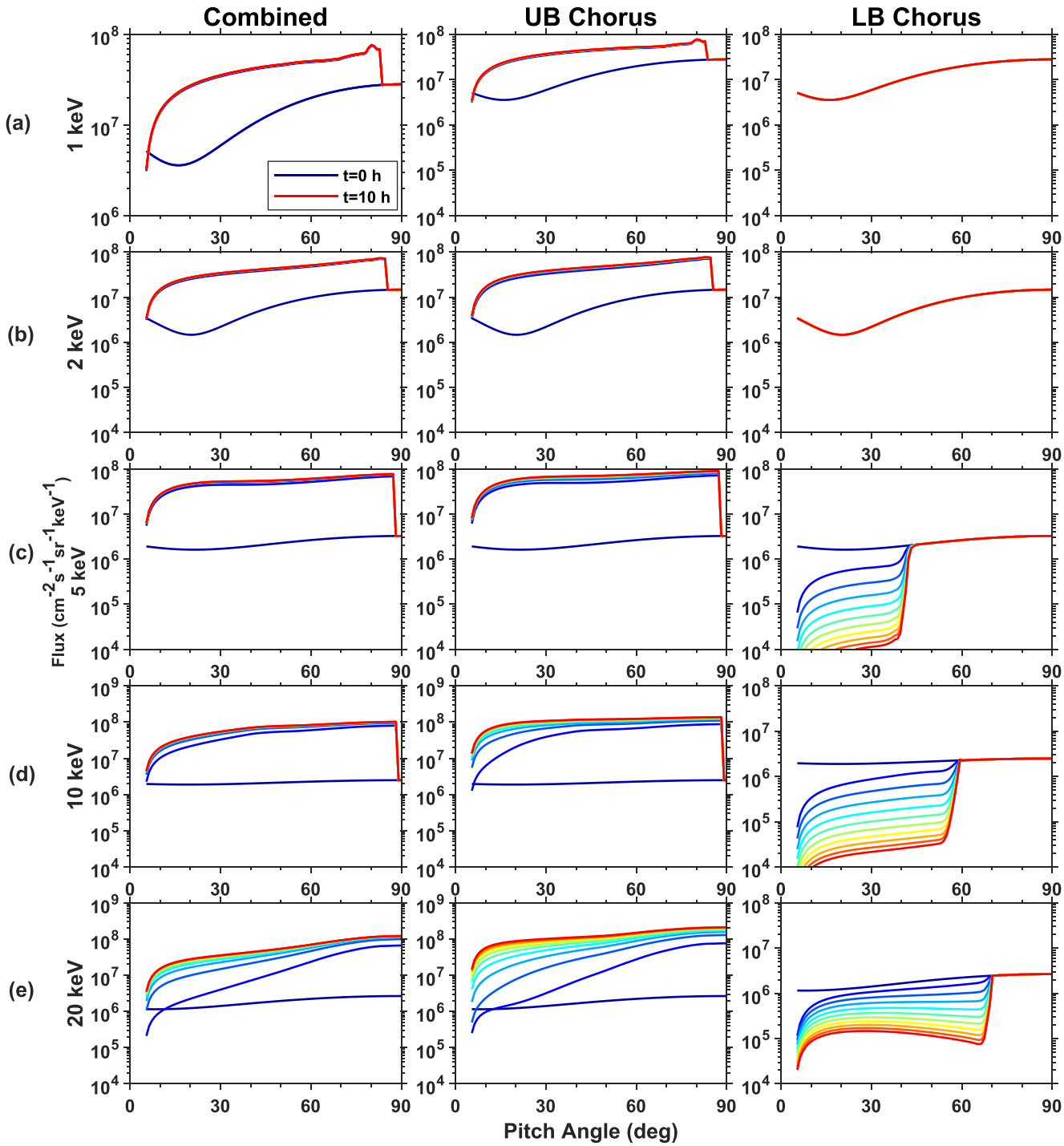

Figure 4. The evolution of electron fluxes at $L = 4$ at energies of (a) 1 keV, (b) 2 keV, (c) 5 keV, (d) 10 keV, and (e) 20 keV. From left to right, columns are the results of the combined effect of upper band chorus and lower band chorus, only upper band chorus, and only the lower band chorus, respectively. Results are displayed every 1 hr in different colors (from blue to red) for the entire 10 hr of the simulation.

5. Discussions

In this study, we present an observation of a strong morning-side diffuse aurora associated with intense chorus waves that occurred during the substorm, through conjugate observations from the DMSP F17 spectrometer and the RBSP-b wave and particle instruments. For this event, we performed a detailed quantitative analysis of the

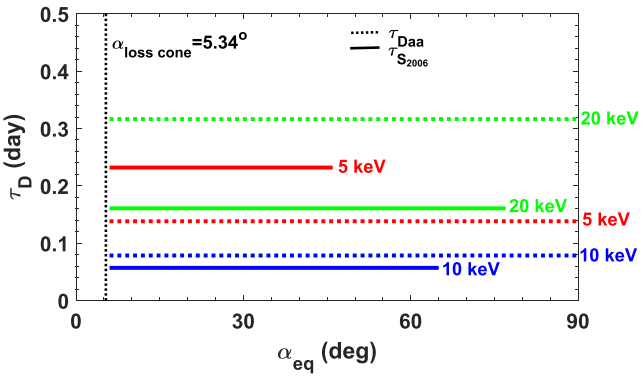

Figure 5. The lifetime (τ_D) of electrons with energies of 5 keV (red lines), 10 keV (blue lines), and 20 keV (green lines). The τ_{Daa} and $\tau_{S_{2006}}$ shown as dotted lines and solid lines respectively are calculated by reversing $D_{\alpha\alpha}$ at the loss cone and the method outlined in Shprits, Li, and Thorne (2006), respectively.

interaction between chorus waves and particles by calculating the diffusion coefficients, the evolution of electron fluxes, and the electron loss timescales. We have confirmed that the scattering by the chorus waves accounted for a large area of diffuse aurora on the morning-side during the substorm. The lower band chorus and upper band chorus play distinct roles during this process. The lower band chorus shows an obvious pitch angle scattering effect for 5, 10, and 20 keV electrons, but no effect on 1 and 2 keV electrons. While the upper band chorus accelerates electrons at all energies from 1 to 20 keV, the effect is most pronounced on electrons with energies higher than 5 keV. We suggest that while the injected plasma sheet particles are drifting from midnight to the dayside, the lower band chorus changes the pitch angle of these electrons and scatters the electrons to the loss cone in a short time, leading to an enhancement of the diffuse aurora, while the upper band chorus accelerates electrons from low energies to high energies where the lower band chorus can efficiently scatter them, thereby participating in the scattering process.

Ni et al. (2014) showed that the dayside chorus scattering was the dominant contributor to the observed dayside diffuse auroral precipitation during relatively quiet geomagnetic conditions. Compared to Ni et al. (2014), the current study presents observations from the recovery phase of a substorm, and the results show that the chorus wave scattering also plays an important role in diffuse aurora formation by affecting the injected particles that are drifting toward the dayside. Furthermore, we confirmed that for this special event, the lower band chorus is the primary contributor for the scattering of 5–20 keV precipitated electrons. During substorms, the plasma sheet electrons from ∼100 eV to 1 keV are injected into the nightside magnetosphere (DeForest & McIlwain, 1971), and drift from the midnight sector through the dawn to the local noon under the effect of gradient and curvature force, and the injected energetic particles could provide the free energy for the excitation of chorus waves (Tsurutani et al., 1979). When the geomagnetic activity intensifies, the amplitude of the chorus also increases (e.g., Li et al., 2009; Meredith et al., 2003; Wang et al., 2019). If chorus provides the dominant scattering mechanism of plasma sheet electrons in the inner magnetosphere, it is not surprising for us to observe the strong emission of morning-side diffuse aurora during this event. In our case study, the RBSP-b instruments detected intense chorus wave activity and a considerable enhancement of ∼10 keV particles when it first traversed the region with $3.5 < L < 4$ at approximately 0130 UT. However, when the RBSP-b passed through this region on its next orbit, the intensity of observed chorus waves was lower, accompanied by a significant reduction in the population of ∼10 keV particles, as shown in Figure 2. These observational results reflect the results of interaction between the chorus waves and particles, that is, the injection of energetic particles facilitates the excitation of chorus waves, and in turn, these waves influence the behavior of the particles, notably by scattering them into the atmosphere. Shi et al. (2015) concluded that the variations of solar wind dynamic pressure can efficiently modulate the intensity of dayside diffuse aurora, which can be explained by the enhancement of solar wind dynamic pressure leading to favorable conditions for the generation of chorus waves. In our case, we also observed an enhancement of solar wind dynamic pressure before the observation of diffuse aurorae, as shown in Figure 1a. Quantifying the relative contribution of the change in dynamic pressure and the injection of energetic particles to the excitation of chorus waves is left as a subject for a future study.

Thorne et al. (2010) showed that the lower band chorus is the most significant contributor to electron precipitation at higher energies (>7 keV), and that the upper band chorus is more important for energies below ∼3 keV. We note that our calculation of the diffusion coefficients using real spectral data shows that the lower band chorus induces scattering of electrons higher than 5 keV, but has no effect on 1–2 keV electrons, as shown in Figure 4. These results are consistent with the results of Yu et al. (2023), who found that the lower band chorus alone can only cause precipitation of electrons with energies greater than 4 keV. The lifetime of these particles with energies above 5 keV is only a few hours, as shown in Figure 5, which is much shorter than the time required for particles to drift from the nightside to the dayside. This means that these particles rapidly enter the loss cone due to the scattering effect of waves, causing strong diffuse auroral emission on the morning-side. It is worth noting that the shortest lifetimes are obtained for 10 keV electrons, which is consistent with the RBSP-b observation that the electron flux decreases the most is most noticeable at 10 keV, as shown in Figure 2. The lifetimes computed by the reversing $D_{\alpha\alpha}$ at the loss

cone and the formula outlined in Shprits, Li, and Thorne (2006) show a slight difference, which results from very small diffusion coefficients near 90-degree pitch-angle. If there exists other scattering process that helps with transporting near 90° pitch angle, for example, by magnetosonic waves, the estimate of lifetime using the diffusion coefficients near the loss cone can be more realistic. Previous studies suggested that the upper band chorus pitch-angle scatters the 1–10 keV electrons, causing the diffuse aurora (e.g., Inan et al., 1992; Miyoshi et al., 2015; Ni et al., 2008). However, in our simulation results, the net effect of upper band chorus on low energy (1–5 keV) particles is acceleration, as shown in Figure 4. This means that the acceleration caused by upper band chorus waves dominate the loss caused by them. On one hand, upper band chorus waves contribute to the precipitation of electrons with energy lower than 5 keV observed by DMSP by scattering these electrons into their loss cones. On the other hand, the acceleration caused by upper band chorus waves also contributes to the precipitation of electrons with energy higher than 5 keV. Here, combining observation and simulation results, we suggest that the upper band chorus accelerates the low energy electrons to higher energies where they can be efficiently pitch-angle scattered by the lower band chorus. This explains why intense upper band chorus activity is correlated with creation of diffuse aurora, describing the contribution of the upper band chorus as the first step of a two-step process. This conclusion is further supported by the fact that our simulation produces these results while overestimating the contribution from the upper band chorus. The wave distribution in our model is assumed to be constant, therefore, the combined action theoretically exhibits an accelerating effect on electrons at all energy levels, as shown in the first column of Figure 4. However, in a real wave spectrum, the upper band chorus wave quickly weakens at orbit-2, as shown in Figure 2, which means lower band chorus scattering will quickly become the major contributor to electron scattering. This indicates that in order to more conclusively describe the specific roles played by upper band chorus and lower band chorus in the generation of dayside diffuse aurora, more in-depth studies using additional examples of wave and auroral conjugate observations are required.

Moreover, butterfly distributions are produced in the simulation results for electrons <10 keV (see Figures 4a–4d). We attribute this phenomenon to acceleration by the upper band chorus, aligning with findings from previous studies (e.g., Fennell et al., 2014). The Van Allen Probes and Arase observations reveal the swift acceleration of electrons characterized by a butterfly type pitch-angle distribution during interactions with upper band chorus (Fennell et al., 2014; Kurita et al., 2018). Test-particle simulations, utilizing data from the Arase satellite, demonstrated that interactions with upper band chorus induce rapid electron acceleration (Saito et al., 2021). Notably, the varied frequencies of the upper band chorus result in differing levels of accelerated energy. We also noticed that the energy flux spectrum of precipitated electrons has a significant gap at ∼1 keV after ∼10:11:00 UT, as shown in Figure 1d. We consider that this gap corresponds to the precipitation gap in Miyoshi et al. (2015). They have discussed that this precipitation gap may correspond to the resonance energy of the half-gyro frequency where the wave amplitude was small. In addition, for this diffuse auroral event, there also exists some burst of the electron precipitation with energy <1 keV from 10:10:00 to10:11:30 UT. Although our simulation results do not primarily account for electrons with energies below 1 keV, we speculate that the wave-particle interactions to scatter the electrons <1 keV are also necessary.

6. Conclusion

In this study, we present a conjugate observation in details that the occurrence of large-scale of morningside diffuse aurora accompanied by intensive chorus waves during a substorm. Through detailed simulation analysis for this event, we found that the lower band chorus wave scattering plays a main role in forming of the large-scale morningside diffuse aurora with precipitated electron energies higher than 5 keV. While the upper band chorus wave accelerates the particles with lower energy to high energy in this event, so that these particles can also participate in the scattering process to form diffuse auroras. The observations and simulation results for this particular event also provide support for our explanation of the relationship between chorus wave and morningside diffuse auroras. However, further investigations about morningside diffuse aurora and waves are still needed, with more joint satellite and ground-based observations of diffuse aurora and wave spectral.

Data Availability Statement

We would like to thank Johns Hopkins University Applied Physics Laboratory for providing the DMSP/SSUSI data https://ssusi.jhuapl.edu/data_products. The DMSP particle detectors were designed by Dave Hardy of AFRL, and data obtained from JHU/APL http://sd-www.jhuapl.edu/Aurora/. We acknowledge the use of NASA/

GSFC's Space Physics Data Facility's OMNI Web service at https://cdaweb.gsfc.nasa.gov/index.html. The Kp index was provided by GFZ Section 2.3 and downloaded from the World Data Center. We acknowledge the NASA Van Allen Probes and Craig Kletzing (University of Iowa), Harlan *E.* Spence (University of New Hampshire) for use of data, and the data obtained from https://rbspgway.jhuapl.edu/.

Acknowledgments

This work was supported by the National Natural Science Foundation of China (42030101). This work was also supported by the Fundamental Research Funds for the Central Universities ZD2023030. This project has received funding from the European Union's Horizon 2020 research and innovation programme under grant agreement No. 637302 (PAGER) and the Helmholtz-Gemeinshaft (HGF) [https://doi.org/10.13039/501100001656]. Dedong Wang acknowledges the support from the Deutsche Forschungsgemeinschaft (DFG) through the project "Understanding the Properties of Chorus Waves in the Earth's Inner-magnetosphere and Their Effects on Van Allen Radiation Belt Electrons" (Chorus Waves)—WA 4323/5-1. We would like to thank Matyas Szabo-Roberts, for helpful comments on the paper text. We would like to thank the reviewers for their helpful comments and suggestions in improving the manuscript. Open Access funding enabled and organized by Projekt DEAL.

References

Albert, J. M. (2004). Using quasi-linear diffusion to model acceleration and loss from wave-particle interactions. *Space Weather*, *2*(9), S09S03. https://doi.org/10.1029/2004SW000069

Baker, D. N. (2021). Wave–particle interaction effects in the Van Allen belts. *Earth Planets and Space*, *73*(1), 189. https://doi.org/10.1186/s40623-021-01508-y

Bortnik, J., & Thorne, R. M. (2007). The dual role of ELF/VLF chorus waves in the acceleration and precipitation of radiation belt electrons. *Journal of Atmospheric and Solar-Terrestrial Physics*, *69*(3), 378–386. https://doi.org/10.1016/j.jastp.2006.05.030

Burtis, W. J., & Helliwell, R. A. (1969). Banded chorus—A new type of VLF radiation observed in the magnetosphere by OGO 1 and OGO 3. *Journal of Geophysical Research*, *74*(11), 3002–3010. https://doi.org/10.1029/JA074i011p03002

DeForest, S. E., & McIlwain, C. E. (1971). Plasma clouds in the magnetosphere. *Journal of Geophysical Research*, *76*(16), 3587–3611. https://doi.org/10.1029/JA076i016p03587

Elkington, S. R. (2006). A review of ULF interactions with radiation belt electrons. In K. Takahashi, P. J. Chi, R. E. Denton, & R. L. Lysak (Eds.), *Magnetospheric ULF waves: Synthesis and new directions, Geophysical Monograph Series*. https://doi.org/10.1029/169GM12

Feldstein, Y. I. (1973). Auroral oval. *Journal of Geophysical Research*, *78*(7), 1210–1213. https://doi.org/10.1029/JA078i007p01210

Feldstein, Y. I. (2016). The discovery and the first studies of the auroral oval: A review. *Geomagnetism and Aeronomy*, *56*(2), 129–142. https://doi.org/10.1134/S0016793216020043

Feldstein, Y. I., & Galperin, Y. I. (1985). The auroral luminosity structure in the high-latitude upper atmosphere: Its dynamics and relationship to the large-scale structure of the Earth's magnetosphere. *Review of Geophysics*, *23*(3), 217–275. https://doi.org/10.1029/RG023i003p00217

Feng, H.-T., Han, D.-S., Qiu, H.-X., Shi, R., Yang, H.-G., & Zhang, Y.-L. (2021). Observational properties of 15MLT-PCA in the Southern Hemisphere and the switching effects of IMF B_y on 15MLT-PCA occurrence. *Journal of Geophysical Research: Space Physics*, *126*(12), e2021JA029140. https://doi.org/10.1029/2021JA029140

Fennell, J. F., Roeder, J. L., Kurth, W. S., Henderson, M. G., Larsen, B. A., Hospodarsky, G., et al. (2014). Van Allen Probes observations of direct wave-particle interactions. *Geophysical Research Letters*, *41*(6), 1869–1875. https://doi.org/10.1002/2013GL059165

Frank, L. A., & Ackerson, K. L. (1972). Local-time survey of plasma at low altitudes over the auroral zones. *Journal of Geophysical Research*, *77*(22), 4116–4127. https://doi.org/10.1029/JA077i022p04116

Funsten, H. O., Skoug, R. M., Guthrie, A. A., MacDonald, E. A., Baldonado, J. R., Harper, R. W., et al. (2013). Helium, Oxygen, Proton, and Electron (HOPE) Mass spectrometer for the radiation belt storm probes mission. *Space Science Reviews*, *179*(1–4), 423–484. https://doi.org/10.1007/s11214-013-9968-7

Gao, X., Chen, L., Li, W., Lu, Q., & Wang, S. (2019). Statistical results of the power gap between lower-band and upper-band chorus waves. *Geophysical Research Letters*, *46*(8), 4098–4105. https://doi.org/10.1029/2019GL082140

Han, D., Chen, X.-C., Liu, J.-J., Qiu, Q., Keika, K., Hu, Z.-J., et al. (2015). An extensive survey of dayside diffuse aurora based on optical observations at Yellow River Station. *Journal of Geophysical Research: Space Physics*, *120*(9), 7447–7465. https://doi.org/10.1002/2015ja021699

Han, D.-S., Feng, H.-T., Zhang, H., Zhou, S., & Zhang, Y.-L. (2020). A new type of polar cap arc observed in the ∼1500 MLT sector: 1. Northern hemisphere observations. *Geophysical Research Letters*, *47*(20), e2020GL090261. https://doi.org/10.1029/2020GL090261

Hardy, D. A., Schmitt, L. K., Gussenhoven, M. S., Marshall, F. J., Yeh, H. C., Shumaker, T. L., et al. (1984). *Precipitating electron and ion-detectors (SSJ/4) for the block 5D/flights 6–10 DMSP satellites: Calibration and data presentation*. Air Force Geophys Lab, HanscomAir Force Base, Bedford, Mass.

Horne, R. B., Christiansen, P. J., Gough, M. P., Rönnmark, K., Johnson, J. F. E., Sojka, J., & Wrenn, G. L. (1981). Amplitude variations of electron cyclotron harmonic waves. *Nature*, *294*(5839), 338–340. https://doi.org/10.1038/294338a0

Horne, R. B., & Thorne, R. M. (2000). Electron pitch angle diffusion by electrostatic electron cyclotron harmonic waves: The origin of pancake distributions. *Journal of Geophysical Research*, *105*(A3), 5391–5402. https://doi.org/10.1029/1999ja900447

Horne, R. B., Thorne, R. M., Meredith, N. P., & Anderson, R. R. (2003). Diffuse auroral electron scattering by electron cyclotron harmonic and whistler mode waves during an isolated substorm. *Journal of Geophysical Research*, *108*(A7), 1920. https://doi.org/10.1029/2002JA009736

Hosokawa, K., Kullen, A., Milan, S., Reidy, J., Zou, Y., Frey, H. U., et al. (2020). Aurora in the polar cap: A review. *Space Science Reviews*, *216*(1), 15. https://doi.org/10.1007/s11214-020-0637-3

Inan, U. S., Chiu, Y. T., & Davidson, G. T. (1992). Whistler-mode chorus and morningside aurorae. *Geophysical Research Letters*, *19*(7), 653–656. https://doi.org/10.1029/92gl00402

Kennel, C. F., Scarf, F. L., Fredricks, R. W., McGehee, J. H., & Coroniti, F. V. (1970). VLF electric field observations in the magnetosphere. *Journal of Geophysical Research*, *75*(31), 6136–6152. https://doi.org/10.1029/ja075i031p06136

Kessel, R. L., Fox, N. J., & Weiss, M. (2013). The radiation belt storm probes (RBSP) and space weather. *Space Science Reviews*, *179*(1–4), 531–543. https://doi.org/10.1007/s11214-012-9953-6

Kletzing, C. A., Kurth, W. S., Acuna, M., MacDowall, R. J., Torbert, R. B., Averkamp, T., et al. (2013). The electric and magnetic field instrument suite and integrated science (EMFISIS) on RBSP. *Space Science Reviews*, *179*(1–4), 127–181. https://doi.org/10.1007/s11214-013-9993-6

Kozyra, J. U., Rasmussen, C. E., Miller, R. H., & Lyons, L. R. (1994). Interaction of ring current and radiation belt protons with ducted plasmaspheric hiss: 1. Diffusion coefficients and timescales. *Journal of Geophysical Research*, *99*(A3), 4069–4084. https://doi.org/10.1029/93ja01532

Kullen, A. (2012). Transpolar Arcs: Summary and recent results. In A. Keiling, E. Donovan, F. Bagenal, & T. Karlsson (Eds.), *Auroral Phenomenology and magnetospheric processes: Earth and other Planets*. https://doi.org/10.1029/2011GM001183

Kurita, S., Miyoshi, Y., Kasahara, S., Yokota, S., Kasahara, Y., Matsuda, S., et al. (2018). Deformation of electron pitch angle distributions caused by upper band chorus observed by the Arase satellite. *Geophysical Research Letters*, *45*(16), 7996–8004. https://doi.org/10.1029/2018GL079104

Li, W., & Hudson, M. (2019). Earth's Van Allen radiation belts: From discovery to the Van Allen Probes Era. *Journal of Geophysical Research: Space Physics*, *124*(11), 8319–8351. https://doi.org/10.1029/2018JA025940

Li, W., Thorne, R. M., Angelopoulos, V., Bortnik, J., Cully, C. M., Ni, B., et al. (2009). Global distribution of whistler-mode chorus waves observed on the THEMIS spacecraft. *Geophysical Research Letters*, *36*(9), L09104. https://doi.org/10.1029/2009GL037595

Liang, J., Ni, B., Spanswick, E., Kubyshkina, M., Donovan, E. F., Uritsky, V. M., et al. (2011). Fast earthward flows, electron cyclotron harmonic waves, and diffuse auroras: Conjunctive observations and a synthesized scenario. *Journal of Geophysical Research*, *116*(A12), A12220. https://doi.org/10.1029/2011JA017094

Liang, J., Uritsky, V., Donovan, E., Ni, B., Spanswick, E., Trondsen, T., et al. (2010). THEMIS observations of electron cyclotron harmonic emissions, ULF waves, and pulsating auroras. *Journal of Geophysical Research*, *115*(A10), A10235. https://doi.org/10.1029/2009JA015148

Lou, Y., Cao, X., Ni, B., Tu, W., Gu, X., Fu, S., et al. (2021). Diffuse auroral electron scattering by electrostatic electron cyclotron harmonic waves in the dayside magnetosphere. *Geophysical Research Letters*, *48*(5), e2020GL092208. https://doi.org/10.1029/2020GL092208

Lui, A. T. Y., Anger, C. D., Venkatesan, D., Sawchuk, W., & Akasofu, S.-I. (1975). The topology of the auroral oval as seen by the ISIS-2 scanning auroral photometer. *Journal of Geophysical Research*, *80*(13), 1795–1804. https://doi.org/10.1029/JA080i013p01795

Lui, A. T. Y., Perreault, P., Akasofu, S. I., & Anger, C. D. (1973). The diffuse aurora. *Planetary and Space Science*, *21*(5), 857–858. https://doi.org/10.1016/0032-0633(73)90102-5

Lyons, L. R. (1974). Electron diffusion driven by magnetospheric electrostatic waves. *Journal of Geophysical Research*, *79*(4), 575–580. https://doi.org/10.1029/JA079i004p00575

Lyons, L. R., & Thorne, R. M. (1973). Equilibrium structure of radiation belt electrons. *Journal of Geophysical Research*, *78*(13), 2142–2149. https://doi.org/10.1029/ja078i013p02142

Ma, Q., Li, W., Bortnik, J., Kletzing, C. A., Kurth, W. S., Hospodarsky, G. B., & Wygant, J. R. (2019). Global survey and empirical model of fast magnetosonic waves over their full frequency range in Earth's inner magnetosphere. *Journal of Geophysical Research: Space Physics*, *124*(10), 270–282. https://doi.org/10.1029/2019JA027407

Meredith, N. P., Horne, R. B., Thorne, R. M., & Anderson, R. R. (2003). Favored regions for chorus-driven electron acceleration to relativistic energies in the Earth's outer radiation belt. *Geophysical Research Letters*, *30*(16), 1871. https://doi.org/10.1029/2003GL017698

Meredith, N. P., Johnstone, A. D., Szita, S., Horne, R. B., & Anderson, R. R. (1999). "Pancake" electron distributions in the outer radiation belts. *Journal of Geophysical Research*, *104*(A6), 12431–12444. https://doi.org/10.1029/1998JA900083

Min, K., Lee, J., Keika, K., & Li, W. (2012). Global distribution of EMIC waves derived from THEMIS observations. *Journal of Geophysical Research*, *117*(A5), A05219. https://doi.org/10.1029/2012JA017515

Miyoshi, Y., Saito, S., Seki, K., Nishiyama, T., Kataoka, R., Asamura, K., et al. (2015). Relation between fine structure of energy spectra for pulsating aurora electrons and frequency spectra of whistler mode chorus waves. *Journal of Geophysical Research: Space Physics*, *120*(9), 7728–7736. https://doi.org/10.1002/2015JA021562

Ni, B., Bortnik, J., Nishimura, Y., Thorne, R. M., Li, W., Angelopoulos, V., et al. (2014). Chorus wave scattering responsible for the Earth's dayside diffuse auroral precipitation: A detailed case study. *Journal of Geophysical Research: Space Physics*, *119*(2), 897–908. https://doi.org/10.1002/2013JA019507

Ni, B., Liang, J., Thorne, R. M., Angelopoulos, V., Horne, R. B., Kubyshkina, M., et al. (2012). Efficient diffuse auroral electron scattering by electrostatic electron cyclotron harmonic waves in the outer magnetosphere: A detailed case study. *Journal of Geophysical Research*, *117*(A1), A01218. https://doi.org/10.1029/2011JA017095

Ni, B., & Thorne, R. M. (2012). Recent Advances in understanding the diffuse auroral precipitation: The role of resonant wave-particle interactions. In D. Summers, I. R. Mann, D. N. Baker, & M. Schulz (Eds.), *Dynamics of the Earth's radiation belts and inner magnetosphere*. https://doi.org/10.1029/2012GM001337

Ni, B., Thorne, R. M., Shprits, Y. Y., & Bortnik, J. (2008). Resonant scattering of plasma sheet electrons by whistler-mode chorus: Contribution to diffuse auroral precipitation. *Geophysical Research Letters*, *35*(11), L11106. https://doi.org/10.1029/2008GL034032

Ni, B., Thorne, R. M., Zhang, X., Bortnik, J., Pu, Z., Xie, L., et al. (2016). Origins of the Earth's diffuse auroral precipitation. *Space Science Reviews*, *200*(1–4), 205–259. https://doi.org/10.1007/s11214-016-0234-7

Nishimura, Y., Bortnik, J., Li, W., Thorne, R. M., Lyons, L. R., Angelopoulos, V., et al. (2010). Identifying the driver of pulsating aurora. *Science*, *330*(6000), 81–84. https://doi.org/10.1126/science.1193186

Nishimura, Y., Bortnik, J., Li, W., Thorne, R. M., Ni, B., Lyons, L. R., et al. (2013). Structures of dayside whistler-mode waves deduced from conjugate diffuse aurora. *Journal of Geophysical Research: Space Physics*, *118*(2), 664–673. https://doi.org/10.1029/2012JA018242

Nishimura, Y., Lessard, M. R., Katoh, Y., Miyoshi, Y., Grono, E., Partamies, N., et al. (2020). Diffuse and pulsating aurora. *Space Science Reviews*, *216*(1), 4. https://doi.org/10.1007/s11214-019-0629-3

Orlova, K., & Shprits, Y. Y. (2011). On the bounce-averaging of scattering rates and the calculation of bounce period. *Physics of Plasmas*, *18*(9), 092904. https://doi.org/10.1063/1.3638137

Paxton, L. J., Meng, C.-I., Fountain, G. H., Ogorzalek, B. S., Darlington, E. H., Goldsten, J., & Peacock, K. (1992). SSUSI: Horizon-to-horizon and limb-viewing spectrographic imager for remote sensing of environmental parameters. In *Ultraviolet Technology IV* (Vol. 1764, pp. 161–176). SPIE.

Ripoll, J.-F., Claudepierre, S. G., Ukhorskiy, A. Y., Colpitts, C., Li, X., Fennell, J., & Crabtree, C. (2020). Particle dynamics in the Earth's radiation belts: Review of current research and open Questions. *Journal of Geophysical Research: Space Physics*, *125*(5), e2019JA026735. https://doi.org/10.1029/2019JA026735

Royrvik, O., & Davis, T. N. (1977). Pulsating aurora: Local and global morphology. *Journal of Geophysical Research*, *82*(29), 4720–4740. https://doi.org/10.1029/JA082i029p04720

Saito, S., Kurita, S., Miyoshi, Y., Kasahara, S., Yokota, S., Keika, K., et al. (2021). Data-driven simulation of rapid flux enhancement of energetic electrons with an upper-band whistler burst. *Journal of Geophysical Research: Space Physics*, *126*(4), e2020JA028979. https://doi.org/10.1029/2020JA028979

Shi, R., Han, D., Ni, B., Hu, Z.-J., Zhou, C., & Gu, X. (2012). Intensification of dayside diffuse auroral precipitation: Contribution of dayside whistler-mode chorus waves in realistic magnetic fields. *Annals of Geophysics*, *30*(9), 1297–1307. https://doi.org/10.5194/angeo-30-1297-2012

Shi, R., Hu, Z.-J., Ni, B., Han, D., Chen, X.-C., Zhou, C., & Gu, X. (2015). Modulation of the dayside diffuse auroral intensity by the solar wind dynamic pressure. *Journal of Geophysical Research: Space Physics*, *119*(12), 10092–10099. https://doi.org/10.1002/2014JA020180

Shprits, Y. Y., Elkington, S. R., Meredith, N. P., & Subbotin, D. A. (2008a). Review of modeling of losses and sources of relativistic electrons in the outer radiation belt I: Radial transport. *Journal of Atmospheric and Solar-Terrestrial Physics*, *70*(14), 1679–1693. https://doi.org/10.1016/jjastp.2008.06.008

Shprits, Y. Y., Elkington, S. R., Meredith, N. P., & Subbotin, D. A. (2008b). Review of modeling of losses and sources of relativistic electrons in the outer radiation belt II: Local acceleration and loss. *Journal of Atmospheric and Solar-Terrestrial Physics*, *70*(14), 1694–1713. https://doi.org/10.1016/j.jastp.2008.06.014

Shprits, Y. Y., Li, W., & Thorne, R. M. (2006). Controlling effect of the pitch angle scattering rates near the edge of the loss cone on electron lifetimes. *Journal of Geophysical Research*, *111*(A12), A12206. https://doi.org/10.1029/2006JA011758

Shprits, Y. Y., & Ni, B. (2009). Dependence of the quasi-linear scattering rates on the wave normal distribution of chorus waves. *Journal of Geophysical Research*, *114*(A11), A11205. https://doi.org/10.1029/2009JA014223

Shprits, Y. Y., Subbotin, D., & Ni, B. (2009). Evolution of electron fluxes in the outer radiation belt computed with the VERB code. *Journal of Geophysical Research*, *114*(A11), A11209. https://doi.org/10.1029/2008ja013784

Shprits, Y. Y., Thorne, R. M., Friedel, R., Reeves, G. D., Fennell, J., Baker, D. N., & Kanekal, S. G. (2006). Outward radial diffusion driven by losses at magnetopause. *Journal of Geophysical Research*, *111*(A11), A11214. https://doi.org/10.1029/2006JA011657

Summers, D., Ni, B., & Meredith, N. P. (2007). Timescales for radiation belt electron acceleration and loss due to resonant wave-particle interactions: 2. Evaluation for VLF chorus, ELF hiss, and electromagnetic ion cyclotron waves. *Journal of Geophysical Research*, *112*(A4), A04207. https://doi.org/10.1029/2006JA011993

Swift, D. W. (1981). Mechanisms for auroral precipitation: A review. *Review of Geophysics*, *19*(1), 185–211. https://doi.org/10.1029/rg019i001p00185

Teng, S., Han, D.-S., Liang, J., Zhang, Q., Sun, J., Wang, S., et al. (2023). Conjugate observation of whistler mode chorus, ECH waves and dayside diffuse aurora by MMS and ground-based Yellow River Station. *Journal of Geophysical Research: Space Physics*, *128*(10), e2023JA031865. https://doi.org/10.1029/2023JA031865

Teng, S., Li, W., Tao, X., Shen, X.-C., & Ma, Q. (2019). Characteristics of rising tone whistler mode waves inside the Earth's plasmasphere, plasmaspheric plumes, and plasmatrough. *Geophysical Research Letters*, *46*(13), 7121–7130. https://doi.org/10.1029/2019GL083372

Teng, S., Tao, X., & Li, W. (2019). Typical characteristics of whistler mode waves categorized by their spectral properties using Van Allen Probes observations. *Geophysical Research Letters*, *46*(7), 3607–3614. https://doi.org/10.1029/2019GL082161

Thorne, R. M. (2010). Radiation belt dynamics: The importance of wave-particle interactions. *Geophysical Research Letters*, *37*(22), L22107. https://doi.org/10.1029/2010GL044990

Thorne, R. M., Ni, B., Tao, X., Horne, R. B., & Meredith, N. P. (2010). Scattering by chorus waves as the dominant cause of diffuse auroral precipitation. *Nature*, *467*(7318), 943–946. https://doi.org/10.1038/nature09467

Tsurutani, B. T., & Smith, E. J. (1974). Postmidnight chorus: A substorm phenomenon. *Journal of Geophysical Research*, *79*(1), 118–127. https://doi.org/10.1029/ja079i001p00118

Tsurutani, B. T., Smith, E. J., West, H. I., Jr., & Buck, R. M. (1979). Chorus, energetic electrons and magnetospheric substorms. In P. J. Palmadesso & K. Papadopoulos (Eds.), *Wave instabilities in space plasmas* (pp. 55–62). D. Reidel. https://doi.org/10.1007/978-94-009-9500-0_6

Tsyganenko, N. A. (1989). A magnetospheric magnetic field model with a warped tail current sheet. *Planetary and Space Science*, *37*(1), 5–20. https://doi.org/10.1016/0032-0633(89)90066-4

Wang, D., Shprits, Y. Y., Zhelavskaya, I. S., Agapitov, O. V., Drozdov, A. Y., & Aseev, N. A. (2019). Analytical chorus wave model derived from Van Allen Probe observations. *Journal of Geophysical Research: Space Physics*, *124*(2), 1063–1084. https://doi.org/10.1029/2018JA026183

Wang, D., Yuan, Z., Yu, X., Huang, S., Deng, X., Zhou, M., & Li, H. (2016). Geomagnetic storms and EMIC waves: Van allen probe observations. *Journal of Geophysical Research: Space Physics*, *121*(7), 6444–6457. https://doi.org/10.1002/2015ja022318

Wing, S., & Newell, P. T. (1998). Central plasma sheet ion properties as inferred from ionospheric observations. *Journal of Geophysical Research*, *103*(A4), 6785–6800. https://doi.org/10.1029/97JA02994

Xiao, F., Su, Z., Zheng, H., & Wang, S. (2009). Modeling of outer radiation belt electrons by multidimensional diffusion process. *Journal of Geophysical Research*, *114*(A3), A03201. https://doi.org/10.1029/2008JA013580

Yamamoto, T. (1988). On the temporal fluctuations of pulsating auroral luminosity. *Journal of Geophysical Research*, *93*(A2), 897–911. https://doi.org/10.1029/JA093iA02p00897

Yu, X., Yuan, Z., Yu, J., Wang, D., Deng, D., & Funsten, H. O. (2023). Diffuse auroral precipitation driven by lower-band chorus second harmonics. *Nature Communications*, *14*(1), 438. https://doi.org/10.1038/s41467-023-36095-x